catalysts

MDPI

Article

Efficient and Stable Ni/SBA-15 Catalyst for Dry Reforming of Methane: Effect of Citric Acid Concentration

Mamoona Waris [1,†], Howon Ra [2,†], Sungmin Yoon [1,2], Min-Jae Kim [1,*] and Kyubock Lee [1,*]

[1] Graduate School of Energy Science and Technology, Chungnam National University, 99 Daehak-ro, Yuseong-gu, Daejeon 34134, Republic of Korea; mamoona989@gmail.com (M.W.)
[2] Korea Institute of Energy Research (KIER), 152 Gajeong-ro, Yuseong-gu, Daejeon 34129, Republic of Korea; seojun@kier.re.kr
* Correspondence: minjaek@cnu.ac.kr (M.-J.K.); kyubock.lee@cnu.ac.kr (K.L.); Tel.: +82-42-821-8617 (M.-J.K.); +82-42-821-8610 (K.L.); Fax: +82-42-821-8839 (M.-J.K. & K.L.)
† These authors contributed equally to this study.

Abstract: Citric acid, one of the representative chelate compounds, has been widely used as an additive to achieve the highly dispersed metal-supported catalysts. This study aimed to investigate the effect of citric acid concentration on the preparation of the highly dispersed Ni catalysts on mesoporous silica (SBA-15) for the dry reforming of methane. A series of Ni/SBA-15 catalysts with citric acid were prepared using the acid-assisted incipient wetness impregnation method, and the Ni/SBA-15 catalyst as a reference was synthesized via the impregnation method. First of all, the citric acid addition during the catalyst synthesis step regardless of its concentration resulted in highly dispersed Ni particles of ~4–7 nm in size in Ni/SBA-15 catalysts, which had a superior and stable catalytic performance in the dry reforming of methane (93% of CO_2 conversion and 86% of CH_4 conversion). In addition, the amount of coke formation was much lower in a series of Ni/SBA-15 catalysts with citric acid (~2–5 mg_{coke} $g_{cat}{}^{-1}$ h^{-1}) compared to pristine Ni/SBA-15 catalysts (~22 mg_{coke} $g_{cat}{}^{-1}$ h^{-1}). However, when the concentration of citric acid became higher, the more free NiO species that formed on the SBA-15 support, leading to large Ni particles after the stability test. The addition of citric acid is a very clear strategy for making highly dispersed catalysts, but its concentration needs to be carefully controlled.

Keywords: dry reforming; citric acid; nickel; mesoporous silica; particle size

Citation: Waris, M.; Ra, H.; Yoon, S.; Kim, M.-J.; Lee, K. Efficient and Stable Ni/SBA-15 Catalyst for Dry Reforming of Methane: Effect of Citric Acid Concentration. *Catalysts* **2023**, *13*, 916. https://doi.org/10.3390/catal13060916

Academic Editor: Zhong-Wen Liu

Received: 5 April 2023
Revised: 10 May 2023
Accepted: 18 May 2023
Published: 23 May 2023

1. Introduction

The rapid growth of the world's economy and the increase in population has led to a sharp increase in energy consumption [1–3]. This has resulted in the accumulation of greenhouse gases such as carbon dioxide (CO_2) and methane (CH_4) in the atmosphere, which have become the main cause of climate change [1–3]. This causes extreme natural phenomena, such as severe flooding and drought, which have an amplified impact on the ecosystem, negatively influencing biodiversity [2,3]. To alleviate this global warming and climate change, therefore, scientists have suggested a method by which to utilize CO_2 and CH_4 as resources for syngas (CO and H_2) production, which can be potentially be converted into heavier weight or partially oxidized hydrocarbons [1,2].

The dry reforming of methane (DRM) is the one of the main methods that consumes the two major greenhouse gases (CO_2 and CH_4) in order to produce syngas ($CO_2 + CH_4 \rightarrow 2CO + 2H_2$) [1,2,4]. DRM produces a ratio of H_2/CO that is equal to one, which can be easily utilized in industry [1,2]. For this process, catalysts are an essential entity, as they are responsible for altering the reaction rate, thus improving the syngas production without being consumed [4,5]. DRM reactions can be catalyzed by metals such as Pt, Pd, Ru, Co, and Ni, and they are usually mounted on Al_2O_3, SiO_2, CeO_2, ZrO_2, La_2O_3, and TiO_2 [1,4–12]. It is well known that precious metals are highly active in DRM, but those

expensive noble metals have provoked the search for new catalysts made of low-cost and earth-abundant elements [1,4,5,9]. In addition to the active metals, the properties of the support have a great effect on the dispersion, reducibility, morphology, and oxidation state of the active metal, which influences the final performance of the catalyst [1,4,5,13]. Hence, it is necessary to carefully check the combination between the support and active metal.

According to the literature, controlling the metal particle size is an effective approach by which to design a high-performance catalyst and many efforts have been devoted to achieving a high metal dispersion [1,12,14–16]. Moreover, reducing the particle size could improve the metal support interaction, influencing the oxidation state of the active metal on the support and the catalytic efficiency [16]. The facile method employed to control the Ni particle size uses citric acid as an additive [16,17]. The addition of citric acid during the Ni impregnation step has been reported to be an effective strategy by which to enhance the metal dispersion [16,17]. When a chelate compound (citric acid in this study) is added to the impregnation solution, a large complex cluster is formed around the metal [17]. This cluster repelling the adjacent molecules inhibits the aggregation of metal ions due to the steric hindrance and this effect causes the metal particle to be dispersed better on the catalyst surface [16,17]. However, only a few recent studies have reported the activity of an Ni-supported SBA-15 catalyst in the DRM reaction by tuning the particle size and then the chemical state of the Ni nanoparticles depending on the citric acid concentration.

In this study, mesoporous silica (SBA-15) was selected as the support material, which could highly disperse the Ni particles induced by the addition of citric acid. In this study, the 7 wt.% Ni/SBA-15 catalysts were prepared using a citric acid-assisted incipient wetness impregnation method and a pristine Ni/SBA-15 catalyst was also prepared for reference. The mole ratio of citric acid to Ni was varied with the purpose of simultaneously tuning the Ni particle size and metal support interaction. The physicochemical properties of these catalysts were characterized via XRD, TEM, BET, H_2-TPR, XPS, and TGA, and correlated with the catalytic activity. Through this study, it is expected that the optimum ratio of citric acid for a SBA-15-supported catalyst during the Ni impregnation step will be determined.

2. Results and Discussion

2.1. Fresh Catalyst Characterization

2.1.1. Textural and Structural Properties

XRD analysis was carried out to understand the crystal structure of the as-calcined and as-reduced catalysts, as given in Figure 1. Figure 1a presents the XRD patterns of the as-calcined samples: CA0, CA0.35, CA0.7, and CA1.4. Regardless of the concentration of citric acid, basically, all the samples exhibited a broad peak at 22°, which is attributed to the SBA-15 amorphous silica support. For the CA0 catalyst, it showed the sharp and strong characteristic peaks of NiO (PDF #44-1159) at 37.2°, 43.2°, and 62.9°, while these NiO peaks became very weak in the catalysts, CA0.35, CA0.7 and CA1.4. This implied that the particle size of Ni was decreased by the addition of citric acid [17–19]. Figure 1b plots the XRD peaks of the as-reduced samples with a reduction process under a 4% H_2/N_2 atmosphere for 2 h at 800 °C. The diffraction patterns ascribed to the mesoporous SBA-15 silica were similar to those of the as-calcined samples. Different from the XRD peaks of the as-calcined catalysts, new characteristic peaks at 44.5°, 51.8°, and 76.3° were observed for all the reduced samples, attributed to metallic Ni [18,20]. This means that the NiO in mesoporous SBA-15 was successfully reduced to metallic Ni during the reduction process. Moreover, it was revealed that the Ni characteristic peaks of CA0.35, CA0.7, and CA1.4 were not highly developed compared to those of CA0 after reduction, indicating that nickel nitrate impregnated with citric acid would form small Ni nanoparticles on the SBA-15 support with high thermal stability [19,21]. Table 1 summarizes the average particle size and dispersion of Ni, estimated by H_2 pulse chemisorption, and these results indicated that the addition of citric acid influenced the particle size of Ni, which corresponded well to the XRD analysis.

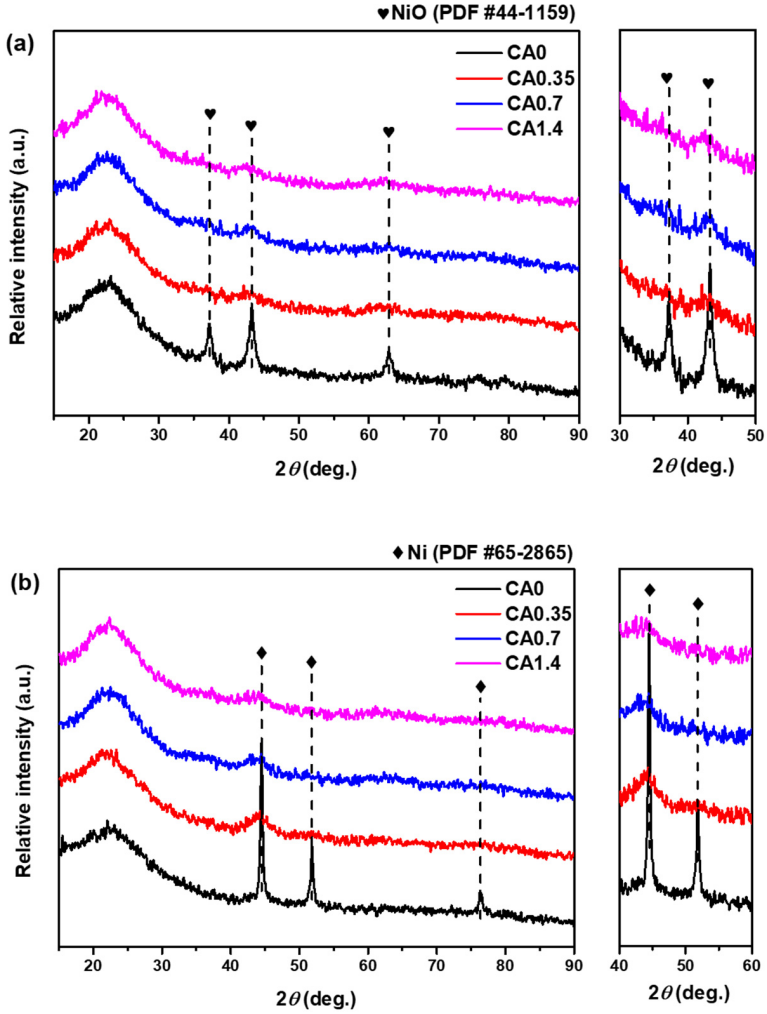

Figure 1. XRD spectra obtained for Ni/SBA-15 (CA0) and the series of Ni/SBA-15 with citric acid (CA0.35, CA0.7, and CA1.4) catalysts: as-prepared (**a**) and as-reduced (**b**) catalysts.

Table 1. Textural properties of as-reduced Ni/SBA-15 and a series of Ni/SBA-15 with citric acid.

Samples	Average Particle Size of Ni [a] (nm)	Ni Dispersion [a] (%)	BET Surface Area [b] (m^2 g^{-1})	Pore Volume [b] (cm^3 g^{-1})	Ni contents [c] (wt.%)
SBA-15	-	-	824.03	0.9029	
CA0	49.3	2.05	584.54	0.6449	7.28
CA0.35	8.2	12.23	517.81	0.5837	6.02
CA0.7	7.6	13.29	449.34	0.5545	7.7
CA1.4	7.3	13.83	455.26	0.5028	8.76

[a] Estimated by H_2 pulse chemisorption. [b] Estimated by N_2 isotherm. [c] Estimated by ICP-MS.

TEM analysis was conducted to visually observe the Ni particles on the as-reduced catalysts. Prior to this analysis, the samples were dispersed in ethanol using ultra-sonication and loaded homogeneously on the copper grid to obtain detailed images, which clearly show the mesopore structures of SBA-15 as well as the Ni particles. Figure 2a–d presents the TEM images of the as-reduced Ni/SBA-15 (CA0) and the series of Ni/SBA-15 with citric acid (CA0.35, CA0.7, and CA1.4) catalysts. The CA0 catalyst had bulk Ni particles placed also on the outer surface of the SBA-15 (Figure 2a), whereas the catalysts synthesized by the addition of citric acid (CA0.35, CA0.7, and CA1.4) show much smaller Ni particles located inside of the SBA-15 pore structure (Figure 2b–d). This result clearly indicates that the

addition of citric acid during the metal impregnation process helps to form nanoparticles of metallic Ni, which are small enough to be located inside of the SBA-15 pore [21]. The size and distribution of the metallic Ni over SBA-15 were dependent on the citric acid addition and concentration, shown in Figure 2e–h. In the case of the CA0, the Ni particle size was widely varied from 10 to 30 nm (d_{ave} = 16.7 nm), whereas a very narrow size distribution of Ni particles was observed over CA0.35, CA0.7, and CA1.4 (d_{ave} = 4.45, 4.78, and 7.01 nm, respectively).

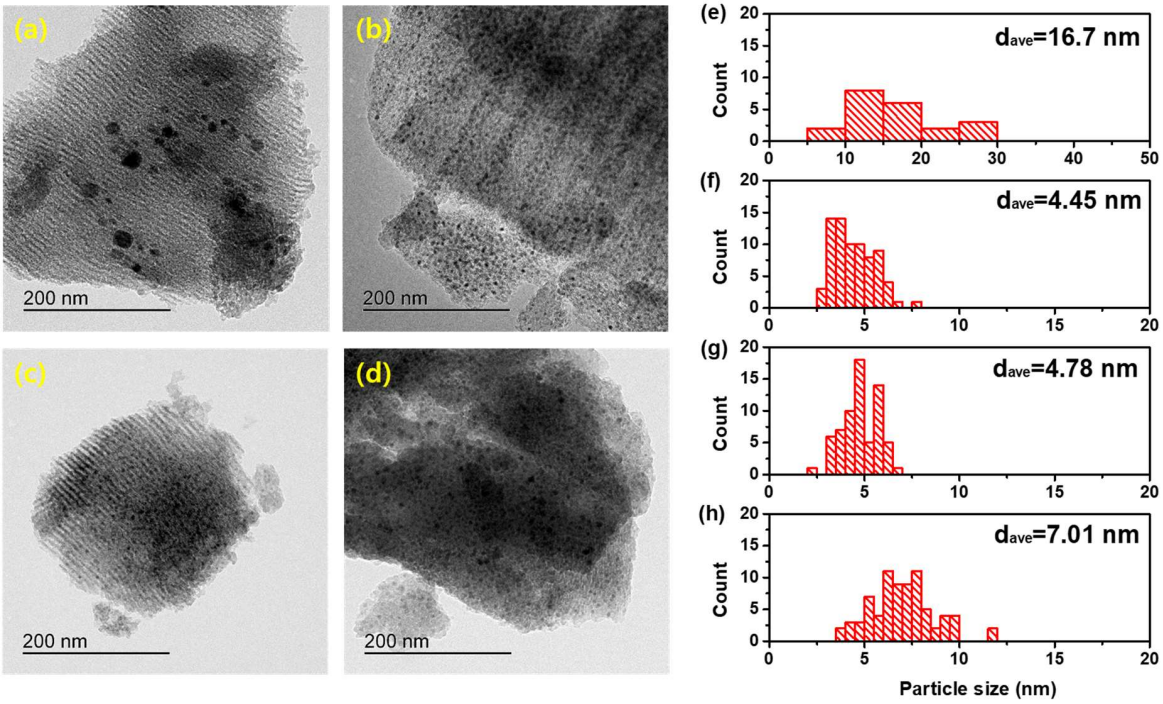

Figure 2. TEM images (**a**–**d**) and diameter distributions of Ni nanoparticle (**e**–**h**) on the as-reduced catalysts: the Ni/SBA-15 (CA0 (**a**,**e**)) and a series of Ni/SBA-15 with citric acid (CA0.35 (**b**,**f**), CA0.7 (**c**,**g**), and CA1.4 (**d**,**h**)) catalysts.

In these TEM images (Figure 2a–d), interestingly, the only thing changed by the citric acid was the particle size of Ni and there were no discernible changes in the support structure with the addition of citric acid. For a better understanding of the support structure, a nitrogen adsorption–desorption analysis was conducted over the as-reduced samples. Figure 3 exhibits the nitrogen isotherms and pore size distributions of the as-reduced samples. As given in Figure 3a, all the samples have the typical Type-IV isotherm, with obvious hysteresis in the range of 0.4–0.7 P/P_0 [19,21]. Figure 3b presents the pore-size distribution of each sample estimated using the BJH method. All the samples possessed mesopores of identical sizes, with diameters ranging from 2 to 8 nm, indicating that the pore structure and the size of the SBA-15 support were identical regardless of the addition of citric acid and its concentration, corresponding well to the TEM analysis. Table 1 presents the textural properties of the Ni/SBA-15 and the series of Ni/SBA-15 with citric acid, as estimated by the N_2 adsorption–desorption method. The BET surface area and the pore volume of CA0 were 584.54 $m^2\ g^{-1}$ and 0.6449 $cm^3\ g^{-1}$, respectively. Those numbers were decreased with the addition of citric acid (BET surface area = 517.81 $m^2\ g^{-1}$ and the pore volume = 0.5837 $cm^3\ g^{-1}$ for CA0.35), and furthermore, a higher citric acid concentration (CA0.7 and CA1.4) led a smaller BET surface area and pore volume (BET surface area = 449.34 $m^2\ g^{-1}$ and 455.26 $m^2\ g^{-1}$ and the pore volume = 0.5545 $cm^3\ g^{-1}$ and 0.5028 $cm^3\ g^{-1}$ for CA0.7 and CA1.4, respectively). This result would be due to the fact that Ni nanoparticles induced by the citric acid were placed on the inside of the support structure and caused the pore blockage, not because of support structure change.

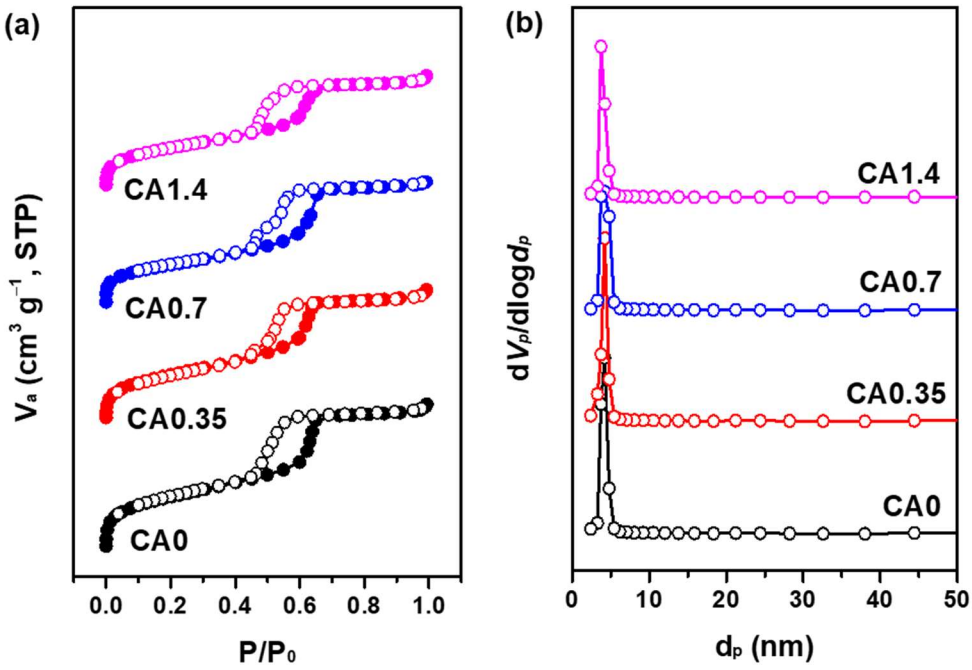

Figure 3. N_2 adsorption/desorption isotherms (**a**) and pore size distribution (**b**) of the as-reduced samples: the Ni/SBA-15 (CA0) and series of Ni/SBA-15 with citric acid (CA0.35, CA0.7, and CA1.4) catalysts.

2.1.2. Reduction Behavior and Oxidation State of Catalysts

H_2-TPR analysis was conducted to examine the reduction behavior of Ni/SBA-15 (CA0, CA0.35, CA0.7, and CA1.4) catalysts (Figure 4). According to the literature, the reduction peak at 250–400 °C is ascribed to the reduction of surface NiO particles, with a poor interaction with the support, and the reduction peak in the temperature range of 400–600 °C is attributed to the reduction of NiO particles in the pore with a strong interaction with the support [14,15,21]. The CA0 had very large peaks for NiO belonging to both the poor and strong interaction with support. In contrast to CA0, the reduction behavior was significantly changed in CA0.35, CA0.7, and CA1.4. The reduction peaks of the surface NiO were clearly decreased but those of the NiO having a strong interaction with the support were relatively developed, indicating that the NiO nanoparticles with a strong metal–support interaction had been formed due to the addition of citric acid [16,17]. In terms of the citric acid concentration, there was one more thing we needed to focus on. That is, the high concentration of citric acid in the impregnation solution that led to the bigger surface NiO having a poor metal–support interaction. According to the literature, it is reported that Ni catalysts with a strong metal–support interaction are essential for the stable catalytic performance and it suppressed the formation of carbon fibers [20]. Therefore, this H_2-TPR result presented that there were different kinds of nickel species induced by the citric acid and it is expected that the catalytic performance for DRM would be very different due to this reduction behavior change.

The XPS experiment investigated the oxidation state of Ni species on the catalyst surface of the as-reduced samples. Curve-fitting for the present analysis was performed after the Shirley-type background subtraction using a combination of Gaussian and Lorentzian functions. Figure 5 shows the Ni $2p_{3/2}$ spectra for Ni/SBA-15 (CA0) and a series of Ni/SBA-15 with citric acid (CA0.35, CA0.7, and CA1.4). The XPS peaks of Ni $2p_{3/2}$ at 851.8–853.0 eV, 855.0–856.6 eV, and 860.0–862.2 eV can be attributed to Ni^0, Ni^{2+}, and the satellite peak, respectively [18,22]. The peak position for Ni species tended to be moved to lower/higher binding energy by the addition of citric acid (CA0.35, CA0.7, and CA1.4), indicating that the citric acid addition influenced the oxidation state of Ni species [16,17]. Table 2 summarizes the peak position of Ni $2p_{3/2}$ over as-reduced catalysts. The Ni^0 and Ni^{2+} peak positions of

CA0.35 were located at the high peak position compared to others. It indicated that nickel species with the strong metal–support interaction could be formed by the addition of a low concentration of citric acid during the Ni metal impregnation step [15,17,23]. According to the H_2-TPR and XPS analysis, the addition of citric acid definitely led to the formation of nickel species with a strong metal–support interaction compared to the catalyst without citric acid, but one more step further, its concentration needs to be carefully controlled.

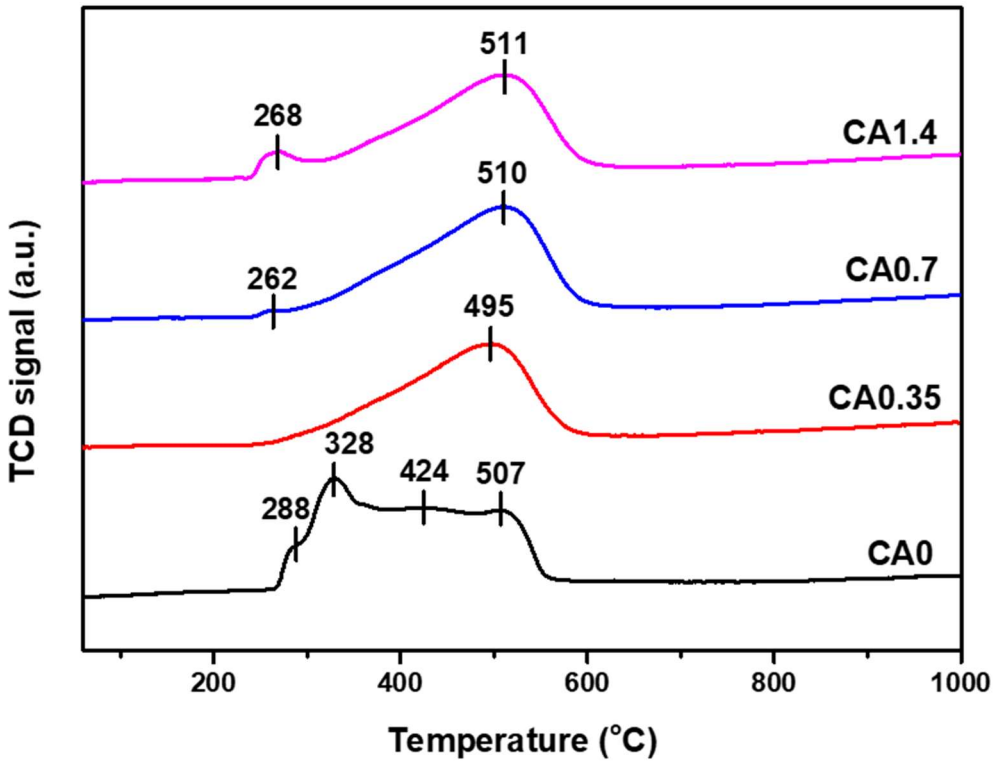

Figure 4. H_2-TPR after pretreatment in He at 50 °C, followed by calcination in 10% O_2/H_2 at 200 °C for 1 h.

Table 2. Ni $2p_{3/2}$ position of as-reduced samples as estimated by XPS analysis.

Samples	Ni $2p_{3/2}$ Peak Position (eV)		
	Sat.	Ni^{2+}	Ni^0
CA0	860.5	854.9	851.8
CA0.35	861.7	856.2	853.0
CA0.7	859.1	854.9	852.2
CA1.4	860.4	855.6	853.0

2.2. Catalytic Activity

To evaluate the catalytic activities of Ni/SBA-15 catalysts (CA0, CA0.35, CA0.7, and CA1.4), DRM reaction tests were conducted at 96,000 $mL \cdot g^{-1}$ h^{-1} of GHSV with a CH_4/CO_2 ratio = 1, changing the reaction temperature from 800 to 600 °C. Figure 6 depicts the CO_2 and CH_4 conversions for CA0, CA0.35, CA0.7, and CA1.4 catalysts as a function of the time-on-stream with changing the reaction temperature. Basically, the conversion of CO_2 was slightly higher than that of CH_4 because the DRM reaction accompanied a reverse water–gas shift ($H_2 + CO_2 \rightarrow CO + H_2O$) reaction as a side reaction [24]. As given in Figure 6, when the reaction temperature was decreased from 800 °C to 600 °C with an interval of 50 °C, the conversion of CO_2 and CH_4, for all catalysts, was accordingly decreased. This deterioration in the catalyst efficiency was due to the reduction in the reaction energy of the reactant on the catalyst surface with decreasing the reaction temper-

ature. The catalytic performance at 800 °C was almost the same for all catalysts, but the conversion of CO_2 and CH_4 became segregated among the catalysts with a decreasing the reaction temperature. The catalytic performance of CA0 was drastically decreased with decreasing the reaction temperature, while that of CA0.35, CA0.7, and CA1.4 was not and their efficiency was much higher than that of CA0. Among the series of the Ni/SBA-15 catalyst with citric acid, furthermore, CA1.4 had the lowest catalytic performance, indicating that the catalyst impregnated with a high concentration of citric acid does not promise high catalytic efficiency.

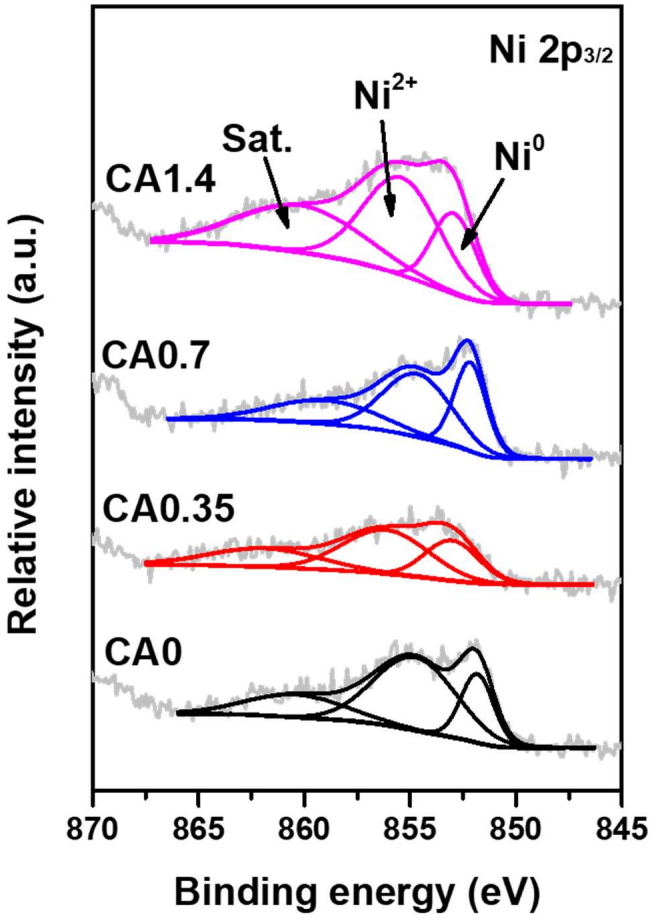

Figure 5. XPS profiles of as-reduced Ni/SBA-15 (CA0) and series of Ni/SBA-15 with citric acid (CA0.35, CA0.7, and CA1.4) catalysts: Ni $2p_{3/2}$.

A stability test was conducted under severe conditions (CO_2/CH_4 = 1, T = 700 °C, and GHSV = 96,000 mL·g^{-1} h^{-1}) for 30 h. Figure 7 exhibits the CO_2 and CH_4 conversion over CA0, CA0.35, CA0.7, CA1.4 catalysts. The H_2/CO ratio for this stability test is presented in Figure S1. The difference in conversion between catalysts was clearly shown. CA0.35, CA0.7, and CA1.4 presented a high efficiency compared to CA0, and among a series of Ni/SBA-15 with citric acid, CA0.35 had the highest conversion of CO_2 and CH_4 for the 30 h DRM reaction. This indicated that the addition of citric acid in a low concentration during the Ni impregnation step led to a high catalytic performance. In the case of CA0, furthermore, the conversion of CO_2 and CH_4 was gradually decreased from 57% to 32% and 38% to 21%, respectively. However, all catalysts impregnated with citric acid showed very stable conversion for CO_2 and CH_4. This clearly indicated that the addition of citric acid in the Ni impregnation step led to stable catalytic efficiency. Table 1S presents the detailed comparison to other catalysts with different condition. It implies the superior catalytic efficiency induced by the citric acid.

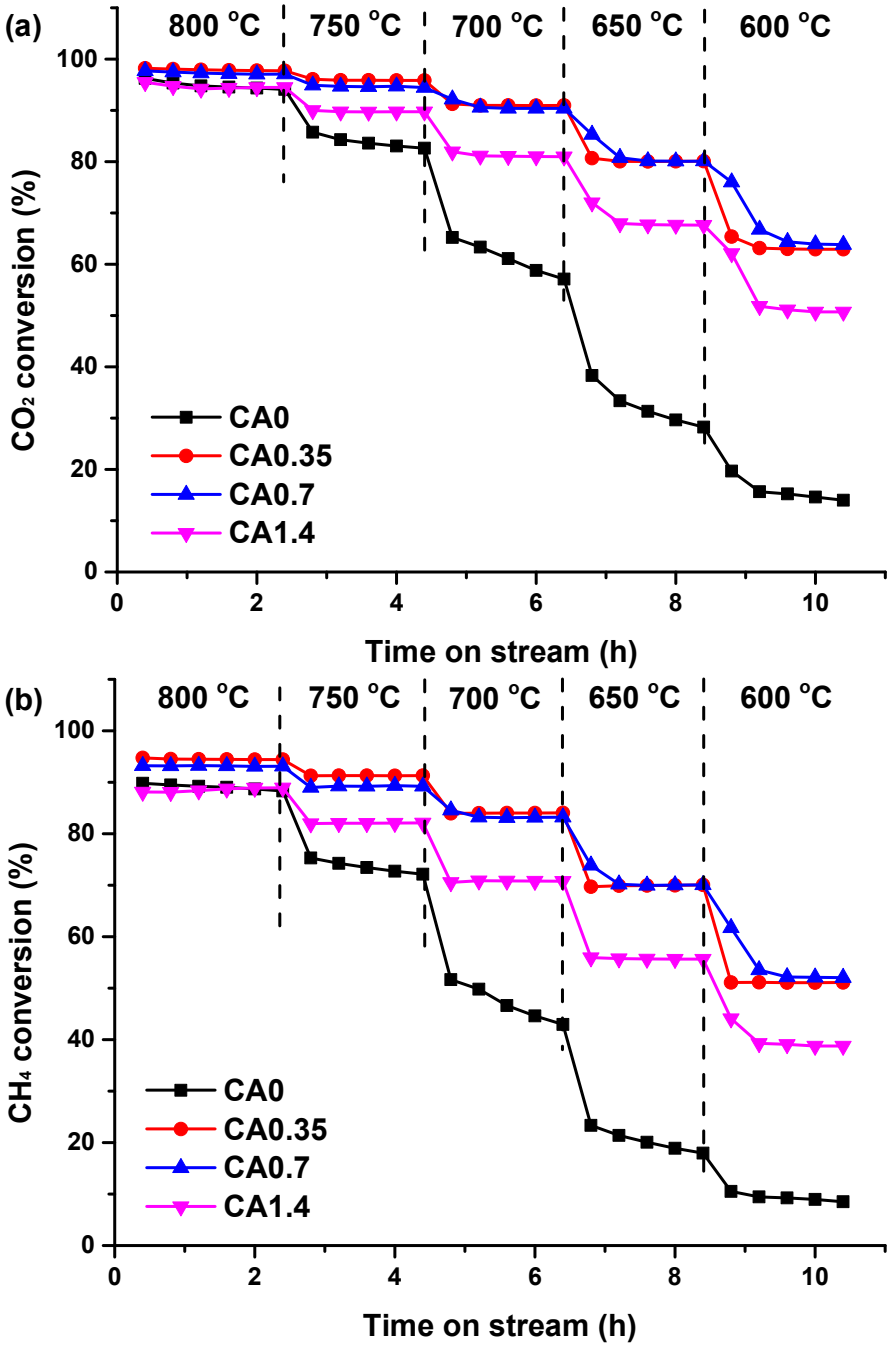

Figure 6. CO_2 (**a**) and CH_4 (**b**) conversion over Ni/SBA-15 (CA0) and series of Ni/SBA-15 with citric acid (CA0.35, CA0.7, and CA1.4) catalysts at different reaction temperatures. Reaction condition: CH_4/CO_2 = 1, P = 1.0 atm, and GHSV = 96,000 $mL \cdot g^{-1}\ h^{-1}$.).

2.3. Spent-Catalyst Characterization

XRD and TEM analysis were performed to investigate the catalyst structure and carbon formation after the 30 h stability test at 700 °C (CO_2/CH_4 = 1 and GHSV = 96,000 $mL \cdot g^{-1}\ h^{-1}$). Figure 8 plots the XRD patterns on the spent catalysts used in DRM. In this XRD analysis, it was difficult to observe the coke formation because the peak position attributed to carbon (PDF #26-1080) overlapped with the diffraction peak of silica, but the structure of nickel and silica was clearly investigated [15,25]. The diffraction patterns attributed to mesoporous SBA-15 silica were similar to those for the fresh samples, indicating the high thermal stability of SBA-15 [14–16]. However, the difference between fresh and spent catalysts was

found in the intensity of characteristic peaks at 44.5°, 51.8°, and 76.3°, ascribed to metallic Ni [18,20]. The peaks of spent catalysts were relatively increased after the DRM reaction compared to those of fresh catalysts, indicating that the size of metallic Ni was grown due to the metal sintering. This was an expected result for all catalysts, but interestingly the metallic Ni peaks for CA0.35 were not significantly increased. This corresponded well to the characterization result, in which there is an optimum concentration of citric acid during the Ni impregnation step for the strong metal–support interaction.

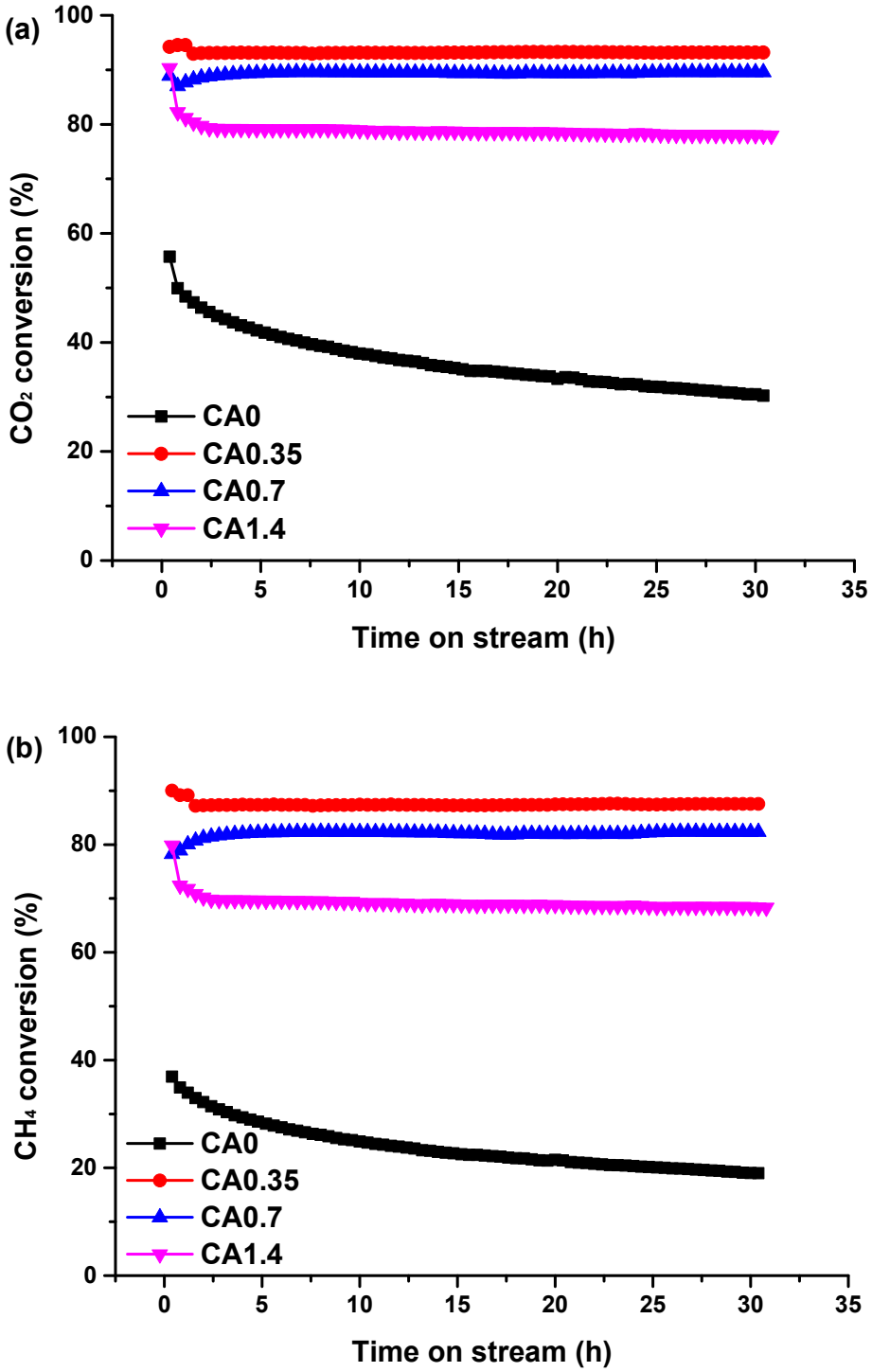

Figure 7. Catalytic stability test for DRM. CO_2 (**a**) and CH_4 (**b**) conversion. Reaction conditions: CH_4/CO_2 = 1, T = 700 °C, P = 1.0 atm, and GHSV = 96,000 mL·g^{-1} h^{-1}.

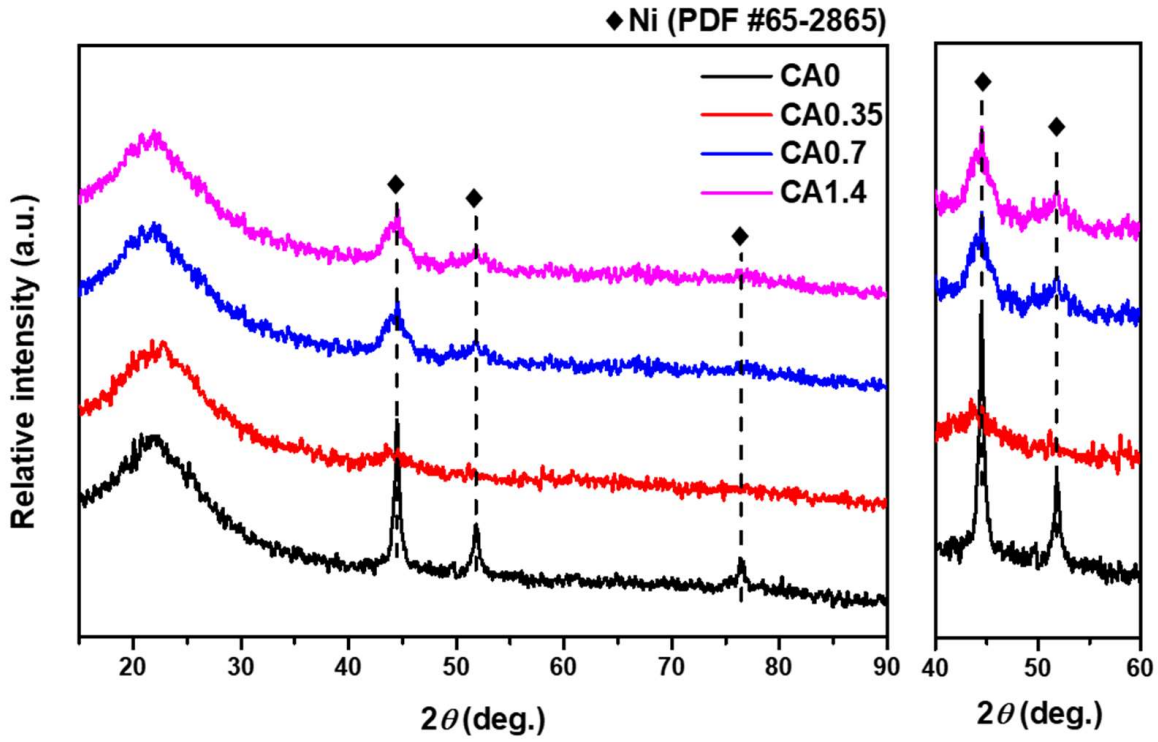

Figure 8. XRD spectra obtained for the spent catalysts: Ni/SBA-15 (CA0) and series of Ni/SBA-15 with citric acid (CA0.35, CA0.7, and CA1.4) catalysts.

Figure 9 shows the TEM images of the spent catalysts. First of all, it is found that there were relatively agglomerated Ni particles in the spent catalysts compared to those in fresh catalysts (Figure 9a–d). The particle size distribution of Ni was plotted on Figure 9e–h. The Ni particles in CA0, CA0.7, and CA1.4 were noticeably grown after the DRM reaction, as confirmed by the XRD, but this growth was small in CA0.35 due to the strong metal–support interaction. This clearly indicated that when the citric acid was added in a low concentration during the impregnation step, most nickel species would have a high thermal stability owing to the strong metal–support interaction, and did not lead to Ni particle agglomeration. In terms of carbon formation on the surface of the catalyst, it was also confirmed that the entangled and randomly grown carbon whiskers were deposited over CA0, CA0.35, CA0.7, and CA1.4 (Figure 9a–d). Some carbon fibers possessed the agglomerated Ni particles detached from the catalyst surface, with this phenomenon mostly observed in CA0 (Figure 9a).

TG analysis was carried out to measure the amount of carbon accumulation formed on the catalyst surface, given in Table 3. The amount of coke accumulation over the reaction time is as follows: CA0 = 21.9 $mg_{coke} \cdot g_{cat}^{-1}\ h^{-1}$, CA0.35 = 2.4 $mg_{coke} \cdot g_{cat}^{-1}\ h^{-1}$, CA0.7 = 4.8 $mg_{coke} \cdot g_{cat}^{-1}\ h^{-1}$, and CA1.4 = 5.1 $mg_{coke} \cdot g_{cat}^{-1}\ h^{-1}$. This supports that adding the citric acid as the chelating agent during catalyst synthesis step would increase the resistance against coke formation and the excess concentration of citric acid rather leads to a negative effect on the catalytic performance.

Table 3. The amount of coke formation on catalyst surface, confirmed by TG analysis.

Samples	Coke Formation ($mg_{coke}\ g_{cat}^{-1}\ h^{-1}$)
CA0	21.9
CA0.35	2.4
CA0.7	4.8
CA1.4	5.1

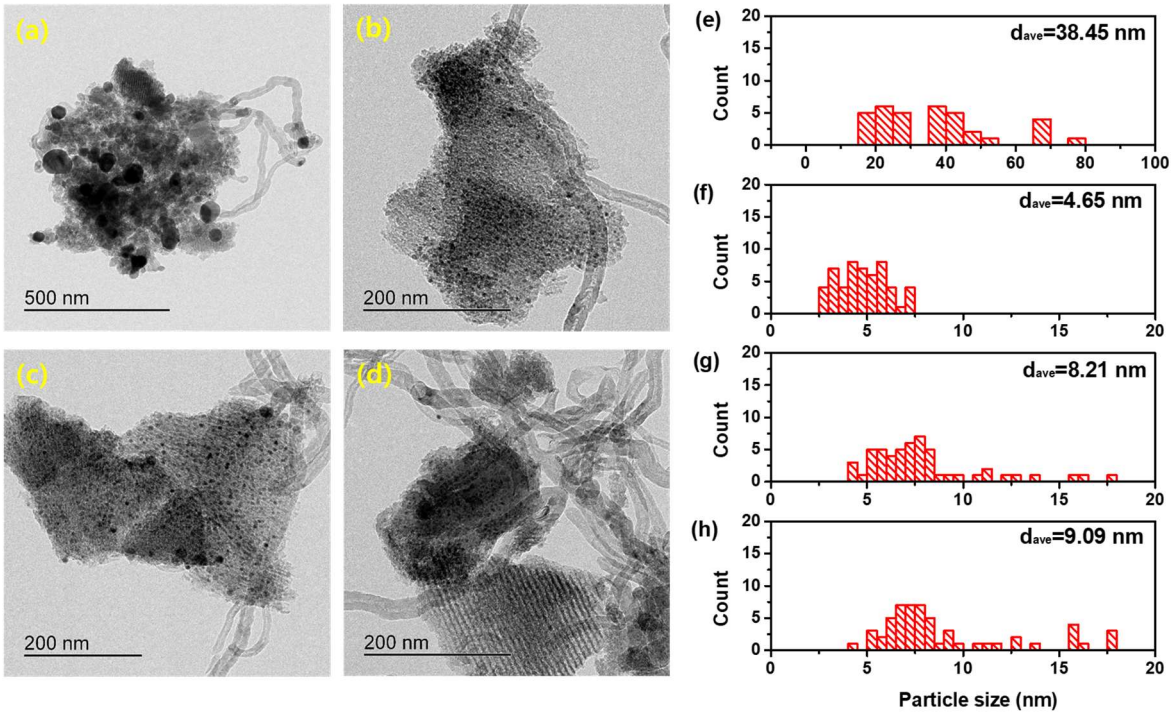

Figure 9. TEM images (**a**–**d**) and diameter distributions of Ni nanoparticle (**e**–**h**) on the spent catalysts: The Ni/SBA-15 (CA0 (**a**,**e**)) and series of Ni/SBA-15 with citric acid (CA0.35 (**b**,**f**), CA0.7 (**c**,**g**), and CA1.4 (**d**,**h**)) catalysts.

3. Experimental Method

3.1. Materials

Nickel nitrate ($Ni(NO_3)_2 \cdot 6H_2O$, ≥98%, Sigma-Aldrich, St. Louis, MI, USA) and tetraethyl orthosilicate ($Si(OC_2H_5)_4$, ≥97%, Tokyo Chemical Industry Co., Ltd., Tokyo, Japan) were used as the sources of Ni and Si, respectively. A pluronic P123 triblock copolymer ($EO_{20}PO_{70}EO_{20}$, molecular weight = 5800 g mol^{-1}, Sigma-Aldrich) was employed as a structure-directing agent. All of the materials were used as received without any further purification.

3.2. Catalyst Preparation

The mesoporous silica SBA-15 was synthesized using a hydrothermal method. First of all, 10 g of P123 was fully dissolved in 300 mL of 2M hydrogen chloride for 2 h, and then 22 mL of tetraethyl orthosilicate (TEOS) was added to this solution. After vigorously stirring at 40 °C for 24 h, the mixture was transferred to the autoclave for the hydrothermal treatment at 100 °C for 24 h. Afterwards, the obtained precipitate was thoroughly washed with deionized water to remove impurities, dried at 70 °C for 24 h, and subsequently calcined at 650 °C for 6 h.

The nitrate form of nickel was added onto SBA-15 via incipient wetness impregnation (nominal amount of active metal fixed at 7 wt.%) using various concentrations of citric acid (The molar concentration of 0.35, 0.7, and 1.4), and then the synthesized sample was calcined at 400 °C for 4 h. The samples were marked as CA0.35, CA0.7, and CA1.4, respectively. A Ni/SBA-15 catalyst in the absence of citric acid was also prepared using the incipient wetness impregnation method as a reference sample, denoted as CA0.

3.3. Catalyst Characterization

X-ray diffraction (XRD) analysis was carried out using a SmartLab (Rigaku, Corp., Akishima, Japan) at a Cu Kα wavelength, 45 kV, and 200 mA. Transmission electron microscopy (TEM) images were obtained using Tecnai G2 F30 (FEI Co., Hillsboro, OR,

USA) at 300 kV, with sample loading on a holey copper grid coated with carbon. The BET surface area of the catalysts was estimated by N_2 physisorption at −196 °C using a BELSORP-mini (BEL Japan. Inc., Osaka, Japan). The pore size distribution was analyzed in accordance with the Barrett–Joymer–Halenda (BJH) theory. Temperature-programmed reduction/desorption (TPR/TPD) analysis was performed in a BELCAT-II (BEL Japan. Inc.). For the H_2-TPR experiment, 100 mg of a sample was loaded onto a quartz tube and pretreated in a flow of 10% O_2 in He at 200 °C for 1 h. After pretreatment, TPR analysis was conducted in the temperature range of 50–1000 °C using 10% H_2 in Ar balance with a ramping rate of 5 °C min^{-1}. For the H_2-chemisorption experiment, 50 mg of calcined sample was pretreated in 5% H_2/Ar at 800 °C for 2 h and cooled down to 50 °C. Then, H_2 gas was injected in order to perform the chemisorption experiment, assuming that the adsorption stoichiometry of H/Ni = 1. The surface electron state of the reduced samples was investigated using a X-ray photoelectron spectrometer (K-Alpha+, Thermo Scientific, Waltham, MA, USA) equipped with a micro-focused monochromatic Al Kα X-ray source (1486.6 eV) at a constant energy of 50 eV. The XPS spectra were carefully calibrated and aligned using the C 1s transition at 284.6 eV. Thermogravimetric (TG) analysis was carried out using the Labsys TGA EVO (Setaram Instrumentation, Caluire-et-Cuire, France) at temperatures up to 1000 °C in air to estimate the amount of carbon formed on the catalyst surface.

3.4. Catalytic Reaction

The catalytic reaction was performed in a fixed-bed reactor (using a quartz tube of 4 mm in internal diameter). The reaction temperature was controlled using a thermocouple placed at the center of the catalyst bed. Prior to the reaction, a sample was sieved to achieve a uniform particle size. The 75 mg of powder was then in situ reduced at 800 °C for 2 h under a flow of 50 sccm (H_2/N_2 = 1/4) to complete the reduction of active metals. The flow was then switched to the reactant mixture (10 vol% of CO_2 and CH_4 in N_2 balance, CH_4/CO_2 = 1) with P = 1.0 atm. The total GHSV was at 96,000 mL·g^{-1} h^{-1}. The stability test was conducted under the conditions of CH_4/CO_2 = 1, T = 700 °C, P = 1.0 atm, and GHSV = 96,000 mL·g^{-1} h^{-1}. The reactants and products were quantified by on-line micro gas chromatography (GC) using a 3000 MicroGC (Agilent Technologies Inc., Santa Clara, CA, USA) equipped with a thermal conductivity detector. The CH_4 and CO_2 conversion was calculated using the following equation:

$$CH_4 \text{ conversion } (\%) = \frac{[CH_4]_{in} - [CH_4]_{out}}{[CH_4]_{in}} \times 100$$

$$CO_2 \text{ conversion } (\%) = \frac{[CO_2]_{in} - [CO_2]_{out}}{[CO_2]_{in}} \times 100$$

where $[CH_4]_{in}$, $[CO_2]_{in}$, $[CH_4]_{out}$, and $[CO_2]_{in}$ are the inlet and outlet volume flows of CH_4 and CO_2 gas, respectively.

4. Conclusions

In order to investigate the effect that citric acid has as the chelating agent on loading Ni active sites, Ni/SBA-15 and a series of Ni/SBA-15 with citric acid were synthesized using the incipient wetness impregnation method for the DRM reaction and various characterization techniques were conducted to understand the changes in the physicochemical properties. By the addition of citric acid, the Ni dispersion was clearly improved and the size of the Ni particles was decreased, while the concentration of citric acid did not significantly change the Ni particle size. In terms of the metal–support interaction, however, the concentration of citric acid for the Ni impregnation step was highly important. The higher the concentration of citric acid added in the impregnation process, the more nickel particles with a weaker metal–support interaction were produced, confirmed by the H_2-TPR and XPS analysis. These properties were clearly shown in the DRM reaction test.

The CA0.35 catalyst had a high catalytic efficiency for the 30 h stability test, and moreover, it generated the least amount of carbon on the catalyst surface and particle agglomeration was minimized compared to the others. In conclusion, using citric acid as the chelating agent has an influence on the formation of the Ni active site and the concentration is of great importance in the formation of a strong metal–support interaction.

Supplementary Materials: The following supporting information can be downloaded at: https://www.mdpi.com/article/10.3390/catal13060916/s1, Figure S1: Catalytic yield for DRM. Reaction conditions: CH_4/CO_2 = 1, T = 700 °C, P = 1.0 atm, and GHSV = 96,000 $mL \cdot g^{-1}h^{-1}$.). Table S1: Comparison of catalysts used in this work with previous literature. References [26–34] are cited in the supplementary materials.

Author Contributions: M.-J.K.; methodology, M.-J.K. and K.L.; software, M.-J.K.; validation, M.-J.K. and K.L.; formal analysis, M.-J.K.; investigation, S.Y.; resources, K.L.; data curation, M.W.; writing—original draft preparation, M.-J.K.; writing—review and editing, M.-J.K.; visualization, M.-J.K.; supervision, K.L.; project administration, K.L.; funding acquisition, K.L. and H.R. All authors have read and agreed to the published version of the manuscript.

Funding: This work was supported by a National Research Council of Science & Technology (NST) grant by the Korea government (MSIT) (No. CRC-20-02-KIST).

Data Availability Statement: Data is contained within the article or supplementary materials.

Acknowledgments: This acknowledgement is made to a National Research Council of Science & Technology (NST) grant by the Korea government (MSIT), Grant No. CRC-20-02-KIST, for support for this research.

Conflicts of Interest: The authors declare no conflict of interest.

References

1. Abdulrasheed, A.; Jalil, A.A.; Gambo, Y.; Ibrahim, M.; Hambali, H.U.; Shahul Hamid, M.Y. A review on catalyst development for dry reforming of methane to syngas: Recent advances. *Renew. Sustain. Energy Rev.* **2019**, *108*, 175–193. [CrossRef]
2. Cho, H.H.; Strezov, V.; Evans, T.J. A review on global warming potential, challenges and opportunities of renewable hydrogen production technologies. *Sustain. Mater. Technol.* **2023**, *35*, e00567. [CrossRef]
3. Gao, Y.; Jiang, J.; Meng, Y.; Yan, F.; Aihemaiti, A. A review of recent developments in hydrogen production via biogas dry reforming. *Energy Convers. Manag.* **2018**, *171*, 133–155. [CrossRef]
4. Jang, W.-J.; Shim, J.-O.; Kim, H.-M.; Yoo, S.-Y.; Roh, H.-S. A review on dry reforming of methane in aspect of catalytic properties. *Catal. Today* **2019**, *324*, 15–26. [CrossRef]
5. Bhattar, S.; Abedin, M.A.; Kanitkar, S.; Spivey, J.J. A review on dry reforming of methane over perovskite derived catalysts. *Catal. Today* **2021**, *365*, 2–23. [CrossRef]
6. Cho, E.; Lee, Y.-H.; Kim, H.; Jang, E.J.; Kwak, J.H.; Lee, K.; Ko, C.H.; Yoon, W.L. Ni catalysts for dry methane reforming prepared by A-site exsolution on mesoporous defect spinel magnesium aluminate. *Appl Catal. A Gen.* **2020**, *602*, 135166. [CrossRef]
7. Kumari, R.; Sengupta, S. Catalytic CO_2 reforming of CH_4 over $MgAl_2O_4$ supported Ni-Co catalysts for the syngas production. *Int. J. Hydrogen Energy* **2020**, *45*, 22775–22787. [CrossRef]
8. Mizuno, S.C.M.; Braga, A.H.; Hori, C.E.; Santos, J.B.O.; Bueno, J.M.C. Steam reforming of acetic acid over $MgAl_2O_4$-supported Co and Ni catalysts: Effect of the composition of Ni/Co and reactants on reaction pathways. *Catal. Today* **2017**, *296*, 144–153. [CrossRef]
9. Jalali, R.; Rezaei, M.; Nematollahi, B.; Baghalha, M. Preparation of Ni/$MeAl_2O_4$-$MgAl_2O_4$ (Me=Fe, Co, Ni, Cu, Zn, Mg) nanocatalysts for the syngas production via combined dry reforming and partial oxidation of methane. *Renew. Energy* **2020**, *149*, 1053–1067. [CrossRef]
10. Kim, S.S.; Lee, S.M.; Won, J.M.; Yang, H.J.; Hong, S.C. Effect of Ce/Ti ratio on the catalytic activity and stability of Ni/CeO_2-TiO_2 catalyst for dry reforming of methane. *Chem. Eng. J.* **2015**, *280*, 433–440. [CrossRef]
11. Sokolov, S.; Kondratenko, E.V.; Pohl, M.M.; Rodemerch, U. Effect of calcination conditions on time on-stream performance of Ni/La_2O_3-ZrO_2 in low-temperature dry reforming of methane. *Int. J. Hydrogen Energy.* **2013**, *38*, 16121–16132. [CrossRef]
12. Zhang, Y.; Zhang, G.; Liu, J.; Li, T.; Wang, Y.; Zhao, Y.; Li, G.; Zhang, Y. Dry reforming of methane over Ni/SiO_2 catalysts: Role of support structure properties. *Fuel* **2023**, *340*, 127490. [CrossRef]
13. Lee, Y.-L.; Lee, K.; Ko, C.H.; Roh, H.-S. Optimization of nano-catalysts for application in compact reformers. *Chem. Eng. J.* **2020**, *431*, 134299. [CrossRef]
14. Ye, R.-P.; Liao, L.; Reina, T.R.; Liu, J.; Chevella, D.; Jin, Y.; Fan, M.; Liu, J. Engineering Ni/SiO_2 catalysts for enhanced CO_2 methanation. *Fuel* **2021**, *285*, 119151. [CrossRef]

15. Ye, R.-P.; Gong, W.; Sun, Z.; Sheng, Q.; Shi, X.; Wang, T.; Yao, Y.; Razink, J.J.; Lin, L.; Zhou, Z.; et al. Enhanced stability of Ni/SiO_2 catalyst for CO_2 methanation: Derived from nickel phyllosilicate with strong metal-support interactions. *Energy* **2019**, *188*, 116059. [CrossRef]
16. Li, W.; Liu, Y.; Mu, M.; Ding, F.; Liu, Z.; Guo, X.; Song, C. Organic acid-assisted preparation of highly dispersed Co/ZrO_2 catalysts with superior activity for CO_2 methanation. *Appl. Catal. B Environ.* **2019**, *254*, 531–540. [CrossRef]
17. Li, Y.; Men, Y.; Liu, S.; Wang, J.; Wang, K.; Tang, Y.; An, W.; Pan, X.; Li, L. Remarkably efficient and stable Ni/Y_2O_3 catalysts for CO_2 methanation: Effect of citric acid addition. *Appl. Catal. B Environ.* **2021**, *293*, 120206. [CrossRef]
18. Kim, M.-J.; Youn, J.-R.; Kim, H.J.; Seo, M.W.; Lee, D.; Go, K.S.; Lee, K.B.; Jeon, S.G. Effect of surface properties controlled by Ce addition on CO_2 methanation over Ni/Ce/Al_2O_3 catalyst. *Int. J. Hydrogen Energy* **2020**, *45*, 24595–24603. [CrossRef]
19. Kim, M.-J.; Kim, Y.-J.; Lee, S.-J.; Ryu, I.-S.; Kim, H.J.; Kim, Y.; Ko, C.H.; Jeon, S.G. Enhanced catalytic activity of the Rh/γ-Al_2O_3 pellet catalyst for N_2O decomposition using high Rh dispersion induced by citric acid. *Chem. Eng. Res. Des.* **2019**, *141*, 455–463. [CrossRef]
20. Kim, M.-J.; Park, S.J.; Kim, K.D.; Kim, W.; Nam, S.C.; Go, K.S.; Jeon, S.G. Fabrication of carbon nanotube with high purity and crystallinity by methane decomposition over ceria-supported catalysts. *J. Ind. Eng. Chem.* **2023**, *119*, 315–326. [CrossRef]
21. Cho, E.H.; Kim, M.J.; Yoon, B.S.; Kim, Y.J.; Song, D.; Koo, K.Y.; Jung, U.; Jeon, S.-G.; Park, Y.-K.; Ko, C.H. Enhancement in nickel-silica interface generation by surfactant-assisted melt-infiltration: Surfactant selection and application in CO_2 hydrogenation. *Chem. Eng. J.* **2022**, *437*, 135166.
22. Cai, W.; Ye, L.; Zhang, L.; Ren, Y.; Yue, B.; Chen, X.; He, H. Highly Dispersed Nickel-Containing Mesoporous Silica with Superior Stability in Carbon Dioxide Reforming of Methane: The Effect of Anchoring. *Materials* **2014**, *7*, 2340–2355. [CrossRef]
23. Han, B.; Zhao, L.; Wang, F.; Xu, L.; Yu, H.; Cui, Y.; Zhang, J.; Shi, W. Effect of Calcination Temperature on the Performance of the Ni@SiO_2 Catalyst in Methane Dry Reforming. *Ind. Eng. Chem. Res.* **2020**, *59*, 13370–13379. [CrossRef]
24. Bian, Z.; Zhong, W.; Yu, Y.; Wang, Z.; Jiang, B.; Kawi, S. Dry reforming of methane on Ni/mesoporous-Al_2O_3 catalysts: Effect of calcination temperature. *Int. J. Hydrogen Energy* **2021**, *46*, 31041–31053. [CrossRef]
25. Ren, H.-P.; Hao, Q.-Q.; Wang, W.; Song, Y.-H.; Cheng, J.; Liu, Z.-W.; Liu, Z.-T.; Lu, J.; Hao, Z. High-performance Ni–SiO_2 for pressurized carbon dioxide reforming of methane. *Int. J. Hydrogen Energy* **2014**, *39*, 11592–11605. [CrossRef]
26. Liu, H.; Li, Y.; Wu, H.; Takayama, H.; Miyake, T.; He, D. Effects of β-cyclodextrin modification on properties of Ni/SBA-15 and its catalytic performance in carbon dioxide reforming of methane. *Catal. Commun.* **2012**, *28*, 168–173. [CrossRef]
27. Daoura, O.; Boutros, M.; Kaydouh, M.-N.; Massiani, P.; Launay, F.; Hassan, N.E. Supported nickel nanocatalysts for the dry reforming of methane: Effect of SBA-15's pore sizes on the catalytic performances of nickel nanoparticles. In *Nanostructured Catalysts for Environmental Applications*; Dosa, M., Piumetti, M., Eds.; Springer: Berlin, Germany, 2021; pp. 113–126. ISBN 978-3-030-58933-2.
28. Tannous, J.; Karam, L.; Kaydouh, M.N.; El Zakhem, H.; El Hassan, N.; Casale, S. Effect of pore geometry of mesoporous supports on catalytic performances in methane reforming. *MATEC Web Conf.* **2018**, *171*, 8–12. [CrossRef]
29. Karam, L.; El Hassan, N. Advantages of mesoporous silica-based catalysts in methane reforming by CO_2 from kinetic perspective. *J. Environ. Chem. Eng.* **2018**, *6*, 4289–4297. [CrossRef]
30. Chong, C.C.; Cheng, Y.W.; Bukhari, S.N.; Setiabudi, H.D.; Jalil, A.A. Methane dry reforming over Ni/fibrous SBA-15 catalysts: Effects of support morphology (rod-liked F-SBA-15 and dendritic DFSBA-15). *Catal Today* **2021**, *375*, 245–257. [CrossRef]
31. Zhang, Q.; Zhang, T.; Shi, Y.; Zhao, B.; Wang, M.; Liu, Q.; Wang, J.; Long, K.; Duan, Y.; Ning, P. A sintering and carbon-resistant Ni-SBA-15 catalyst prepared by solid-state grinding method for dry reforming of methane. *J. CO_2 Util.* **2017**, *17*, 10–19. [CrossRef]
32. Zhang, Q.; Wang, J.; Ning, P.; Zhang, T.; Wang, M.; Long, K.; Huang, J. Dry reforming of methane over Ni/SBA-15 catalysts prepared by homogeneous precipitation method. *Korean J. Chem. Eng.* **2017**, *34*, 2823–2831. [CrossRef]
33. Kaydouh, M.N.; El Hassan, N.; Davidson, A.; Massiani, P. Optimization of Synthesis Conditions of Ni/SbA-15 Catalysts: Confined Nanoparticles and Improved Stability in Dry Reforming of Methane. *Catalysts* **2021**, *11*, 44. [CrossRef]
34. Qiu, S.; Zhang, Q.; Qiu, W.; Zhang, Q.; Lv, W.; Wang, T.; Zhang, Q.; Ma, L. Simply packaging Ni nanoparticles inside SBA-15 channels by co-impregnation for dry reforming of methane. *RSC Adv.* **2017**, *7*, 24551–24560. [CrossRef]